Chemical Engineering Journal 481 (2024) 148674

Contents lists available at ScienceDirect

Chemical Engineering Journal

journal homepage: www.elsevier.com/locate/cej

Bioinspired phenol-based coatings for medical fabrics against antimicrobial resistance

Jose Bolaños-Cardet [a,b], Daniel Ruiz-Molina [a], Victor J. Yuste [b,c,*], Salvio Suárez-García [a,*]

[a] Catalan Institute of Nanoscience and Nanotechnology (ICN2), CSIC and BIST, 08193 Bellaterra, Spain
[b] Cell Death, Senescence and Survival Group, Departament de Bioquímica i Biologia Molecular and Institut de Neurociències, Facultat de Medicina, Campus de Bellaterra, Universitat Autònoma de Barcelona, 08193 Bellaterra, Spain
[c] Centro de Investigación Biomédica en Red Sobre Enfermedades Neurodegenerativas (C.I.B.E.R.N.E.D.), Campus de Bellaterra, 08193 Bellaterra, Spain

ARTICLE INFO

Keywords:
Bioinspired
Catechol
Coatings
Multi-resistant bacteria
Antimicrobial
Healthcare

ABSTRACT

Multi-resistant pathogens can cause several nosocomial infections that can harm hospital interventions or undermine biological processes. In this scenario, the development of novel and efficient antimicrobial materials is essential for reducing pathogen spread. Though many approaches have been followed with this aim, scalability, safety, and efficiency concerns still hamper their clinical transfer. In this work, we overcome these limitations by co-polymerizing phenolic derivatives with amino-terminal ligands. The resulting coatings are successfully applied to woven and non-woven-based materials used in healthcare: paper, cotton and polypropylene. Moreover, the coatings demonstrate multi-pathway antimicrobial activity against six bacteria (*E. coli*, *P. aeruginosa*, *S. aureus*, methicillin-resistant *S. aureus*, *E. faecalis*, and *B. subtilis*) and two fungi (*C. albicans* and *C. auris*), a fact attributed to i) reactive oxygen species generation over time and ii) protic amino groups exposed on the surface. After 180 min, viable bacteria are reduced by more than 99.9 %, with a comparable decline in fungi after 24 h. As a proof-of-concept, coated commercial band-aids tested on skin *ex vivo* reduced bacterial growth by about 90 %. Considering these results and long-lasting, *in vitro* biocompatibility, scalability and eco-friendly technology, these coatings represent a promising alternative to be applied in healthcare environments, avoiding pathogen spread, infections and antimicrobial resistance.

1. Introduction

The overuse of antibiotics has led to the development of antimicrobial resistance (AMR), a growing threat to public health worldwide [1]. AMR occurs when bacteria change over time and no longer respond to drugs, antibiotics and other related antimicrobial medicines, making infections harder to treat and increasing the risk of pathogen spread, severe illness and death. In fact, the World Health Organization (WHO) and United Nations (UN) have reported that AMR poses a major threat to human health around the world, probably overtaking cancer as the world's leading cause of death by 2050 [1,2,3]. In this scenario, the development of novel and more efficient antibacterial materials has become essential to reduce pathogen spread, thus preventing infections. Of relevance is the control of bacterial populations in health environments such as hospitals and other healthcare units to avoid the so-called nosocomial infections, mainly due to bacterial colonization on biomedical surfaces. Nowadays, this type of infection is the sixth leading cause of death in industrialized countries (much higher in the developing world), specially affecting immunocompromised and intensive care patients (e.g., burns), among others (e.g., chronic pathologies such as diabetes) [4]. Among the different materials that may spread bacterial populations, fabrics represent an integral part of patient care: from the clothes of doctors, surgeons and nurses to medical curtains, bed sheets, pillow coverings, masks, gloves and bandages, which are directly in contact with sutures and wounds. For all these reasons, antibacterial coatings for medical fabrics have become a very active field of research [5].

So far, researchers have developed coatings using metal ions or inorganic antibacterial materials thanks to their broad-spectrum biocidal properties and low probability of inducing resistance [6].

* Corresponding authors at: Cell Death, Senescence and Survival Group, Departament de Bioquímica i Biologia Molecular and Institut de Neurociències, Facultat de Medicina, Campus de Bellaterra, Universitat Autònoma de Barcelona, 08193 Bellaterra, Spain (V.J. Yuste). Catalan Institute of Nanoscience and Nanotechnology (ICN2), CSIC and BIST, 08193 Bellaterra, Spain (S. Suárez-García).
E-mail addresses: victor.yuste@uab.cat (V.J. Yuste), salvio.suarez@icn2.cat (S. Suárez-García).

https://doi.org/10.1016/j.cej.2024.148674
Received 18 October 2023; Received in revised form 23 December 2023; Accepted 8 January 2024
Available online 11 January 2024

Nevertheless, the uncontrolled release of ions, inducing cytotoxic effects due to bioaccumulation and competitive protein complexation, has limited their successful translation to clinics [7]. Other reported antibacterial materials are based on quaternary ammonium salts [8] and antimicrobial peptides [9,10]. Nevertheless, these materials have shown deficiencies in terms of bacterial resistance and a high cost of production. Recently, new antimicrobial materials have been reported and extensively studied based on carbon nanotubes and graphene oxide [11]. However, additional concerns regarding public safety and environmental impacts have arisen. As a result, there is a need for alternative novel antibacterial systems that can overcome these limitations and provide effective and safe antimicrobial activity through efficient and controllable mechanisms.

In this scenario, synthetic antibacterial polymers are attracting special attention [12]. Their rationalized chemical design allows for coatings production with multiple antibacterial pathways and broad antimicrobial activity against different pathogens, while avoiding the induction of severe drug resistance. Especially relevant is the family of catechol-based polymers, a phenolic compound found in natural sources such as mussel adhesive proteins, plants, and fruits [13]. These polymers, including polydopamine (PDA), display universal adhesive properties over several substrates with functional properties such as free radical scavenging, UV shielding, photothermal conversion, and enhanced biocompatibility [14]. More recently, the antibacterial

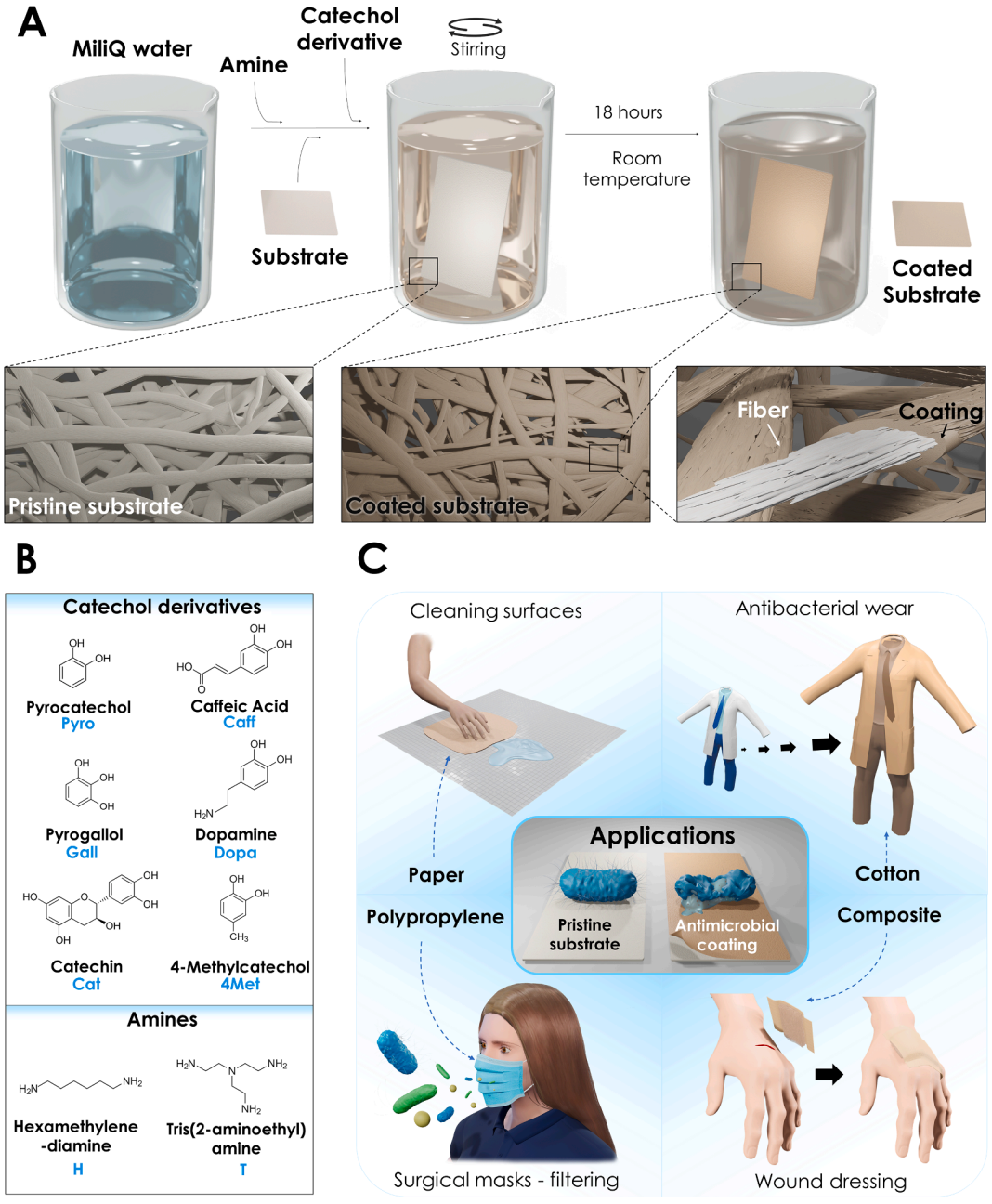

Fig. 1. Bioinspired catechol-amine-based coatings. a) Schematic representation of the coating process of a fiber-based substrate. The used approach allows for the straightforward production of catechol-amine-based coatings under mild conditions using water at room temperature and with the presence of oxygen. After 18 h, functional antimicrobial coatings are obtained ready-to-use. b) Catechol derivatives and amino-based ligands selected for the formation of the bioinspired coatings (in blue their abbreviations). c) The developed antimicrobial coatings could be used in different healthcare applications to avoid microorganism spread, such as: coated paper for surface cleaning, coated cotton and polypropylene to protect patients and personnel and band-aids to avoid infection progression. (For interpretation of the references to color in this figure legend, the reader is referred to the web version of this article.)

properties of catechol-based coatings have also been reported [15]. Catechol oxidation releases reactive oxygen species (ROS) as an effective and broad-spectrum disinfectant [16], while the presence of hydroxyl groups can induce damage of bacterial proteins and cell membranes [17]. Nevertheless, up to now, many of these catechol-based materials have been combined with other antibacterial moieties to produce composites with enhanced antimicrobial activity, using, for example, silver nanoparticles [18], chlorinated catechol moieties [19], or antibacterial compounds such as chitosan [20]. Though, despite its promising landscapes, the antibacterial properties are in its fledgling stage and far from being optimized, requiring in most cases long synthetic methodologies and/or fabrication processes that are still difficult to scale up. Another challenge is to achieve antibacterial activity in the presence of air and humid atmospheres, conditions where the coatings must be functional [21]. For this reason, more efforts must be employed in the design and development of phenol-based materials to improve their antibacterial capabilities.

Herein, we hypothesize that this objective can be achieved with a family of biocompatible coatings produced by the co-polymerization between catechol derivatives and amino-terminal ligands (Fig. 1**a,b**). These coatings, which are synthesized under mild conditions using water at room temperature and fully scalable production protocols (Fig. 1**a**), have already been used to modulate surface properties such as wettability, but not for antimicrobial effects in spite of interest [22]. Based on this, we demonstrate the use of these coatings as efficient antimicrobial materials based on their ability to chemically evolve with time in the presence of air and humid atmospheres, favouring the continuous formation of ROS. Indeed, in addition to the formation of ROS, the synthetic methodology results in an excess of superficial free amino groups that could induce the disruption of pathogen membranes [23]. Interestingly, coated woven and non-woven-based materials commonly used in healthcare environments: paper, cotton, surgical mask and commercial band-aids (Fig. 1**c**), exhibited intrinsic multi-pathway antibacterial activity with fast responses against a broad spectrum of microbial species. This includes microorganisms that have developed resistance to extreme environmental conditions (such as the non-pathogenic *B. subtilis*) as well as pathogens considered as the primary source responsible for many current infections, particularly those acquired in healthcare facilities. These pathogens encompass multi-resistant microorganisms from both Gram-negative (*E. coli* and *P. aeruginosa*) and Gram-positive (*S. aureus*, methicillin-resistant *S. aureus* – MRSA and *E. faecalis*) bacteria. Additionally, these materials have also exhibited efficacy against fungi such as *C. albicans* and *C. auris* [24].

2. Material and methods

All reagents, solvents and kits were purchased and used without further purification from Sigma-Aldrich (Merck, Madrid, Spain) unless otherwise specified. Four substrates were selected: paper, cotton fabric (100 % cotton), surgical mask middle layer (100 % polypropylene) and commercial band-aids (viscose, polyethylene and polypropylene) (Auchan Brand) **(see Supporting Information, Figs. S1 and S5)**. Type 1 ultrapure water from in-house Milli-Q® filtration systems (Millipore, Burlington, MA) was used in all experiments, unless otherwise specified.

2.1. Catechol-amine coating synthesis

The coatings were synthesized by combining different catechol derivatives: pyrocatechol (PYRO), caffeic acid (CAFF), pyrogallol (GALL), catechin (CAT), dopamine (DOPA) and 4-methylcatechol (4MET), and two amino-based ligands: hexamethylenediamine (HMDA, H) and tris (2-aminoethyl)amine (TRIS, T). The coatings obtained and the molarity (mM) of the catechol derivative and amine selected were: **PYRO-H** (10–15), **PYRO-T** (10–22), **CAFF-H** (10–25), **CAFF-T** (10–24), **GALL-H** (10–20), **GALL-T** (10–22), **CAT-H** (10–15), **CAT-T** (10–16), **DOPA-H** (10–20), **DOPA-T** (10–24), **4MET-H** (10–25) and **4MET-T** (10–27) (see Supporting Information, **Table S1**). The selected catechol-derivative and the amine were weighted separately and dissolved in a final volume of 200 ml of Milli-Q® water. Both reagents were mixed and remained under stirring at 300 rpm and room temperature under its complete dissolution. Subsequently, 11 × 5 cm pieces of paper or cotton substrates were introduced into the solution. For band-aids, pieces of 10 × 2 cm were chosen. In the case of polypropylene (directly extracted from the surgical mask middle layer), due to its natural hydrophobicity, ten discs of 9 mm in diameter were cut and stirred at 600 rpm in a final volume of 100 ml. All the recipients were covered with pierced parafilm to allow for oxygen exchange. The reaction only remained fully uncovered when catechin was involved in the synthesis. After 18 h, coated substrates were removed from the solutions, generously cleaned with a continuous flux of distilled water and subsequently dried under vacuum.

2.2. Scanning electron microscopy imaging (SEM)

The morphological characterization of the coatings was determined by scanning electron microscopy (SEM, FEI Quanta 650 FEG, Thermo Fisher Scientific, Eindhoven, The Netherlands) in secondary electron mode with a beam voltage of 10 kV (5 kV in the case of band-aids). Samples were coated with a 5 nm layer of gold/palladium 60/40 layer (Emitech K550X Sputter Coater). The thicknesses of the coatings were measured by previously freezing the samples and breaking in small pieces attached to low profile 45°/90° SEM mount pin.

2.3. Fourier transformed Infra-Red (FT-IR)

Surface FT-IR experiments have been performed with the Hyperion 2000 FT-IR microscope (Bruker Optik GmbH, Ettlingen, Germany) in reflection mode equipped with a nitrogen-cooled mercury–cadmium–telluride (MCT) detector (InfraRed Associates, Inc., Stuart, FL, USA) using a 15 × reflection objective, a gold mirror as a reference and scanning for 30 min with a resolution of 4 cm^{-1}. All the data was treated with OPUS version 7.5 (Bruker) and OriginPro version 8.0988 (OriginLab Corporation, Northampton, MA, USA) software.

2.4. X-ray photoelectron spectroscopy

X-ray photoelectron spectroscopy (XPS) measurements were performed with a Phoibos 150 analyser (SPECS EAS10P GmbH, Berlin, Germany) in ultra-high vacuum conditions (based pressure 10^{-10} mbar, residual pressure around 10^{-7} mbar). A monochromatic Al Kα line was used as X-ray source (1486.6 eV and 300 W). The electron energy analyser was operated with pass energy of 50 eV. The hemispherical analyser was located perpendicular to the sample surface. The data was collected every eV with a dwell time of 0.5 s. A flood gun of electrons, with energy lower than 20 eV, was used to compensate the charge. All the data was treated with CasaXPS version 2.3.17PR1.1 (Casa Software LTD, Teignmouth, UK) and OriginPro version 8.0988 software [25].

2.5. Coating stability

The stability in aqueous media of all the coatings produced by the permutation of the six catechol-derivatives and HMDA or TRIS, was tested. Subsequently to obtain a coated substrate, part of the initial piece was divided into two pieces of 1 × 1 cm. The first one, which remained dry, was considered T = 0, while the other half was stored in a vial with 20 ml of MilliQ® water and maintained under 300 rpm for 60 days (T = 60). Finally, both pieces were compared with SEM pictures to assess the possible changes after the time lapse.

2.6. Contact angle

Changes in wettability were measured before and after the coating.

For that, 1 μl of MilliQ® water was dropped over each condition and the contact angle was measured (Drop Shape Analyzer-DSA25S, KRÜSS GmbH, Hamburg, Germany).

2.7. Zeta potential (ζ-potential)

Surface charge measurements of the coatings were performed using a Zetasizer Nano ZS 3600 (Malvern Instruments, U.K.). The 12 different coatings were isolated by centrifugation (Thermo Scientific™ Sorvall™ Legend™ Micro 17R, centrifuged at 16,200 rcf for 5 min) and washed twice with ultrapure water. The obtained pellet was resuspended in 2 ml ultrapure water and 1 ml introduced in a disposable capillary cell. The data was collected by Zetasizer 7.02 software.

2.8. Bacteria and fungi growth conditions

Six different bacteria and two yeast were selected due to their impact in current human health and relevance in research stated by the WHO and UN [1,2]. *Escherichia coli* (MG 1655) and *Pseudomonas aeruginosa* (PAO1) as representative gram-negative bacteria, while *Staphylococcus aureus* (CECT 86), methicillin-resistant *Staphylococcus aureus* (MRSA, CECT 9951), and *Enterococcus faecalis* (CECT 795) as gram-positive. Specifically, *Bacillus subtilis* (CECT 461) is not considered a pathogenic strain. Nonetheless, the selection of this microorganism was made from a research perspective in order to thoroughly examine the bactericidal properties of the coatings. This choice was based on the microorganism's unique reproduction mechanism, which involves the formation of resilient protective endospores. This protection endows the pathogen with special resistant capabilities to tolerate extreme environmental conditions. Initially, an aliquot from all bacteria was streaked on a 100 mm Petri dish containing Miller's Luria-Bertani (LB) with agar and incubated for 24 h at 37 °C (Forma™ Series II Water-Jacketed CO_2 Incubator) under a saturating humidity atmosphere composed of 95 % air and 5 % CO_2. For each experiment, a single colony was selected and grown in 10 ml of Miller's LB for 24 h at 37 °C. Bacteria cultures were resuspended in NaCl saline solution at 0.9 % and the optical density (OD_{600}) of the suspension was adjusted (Fisherbrand™ Cell Density Meter Model 40) to 0.2 for *E. coli*, 0.15 for *P. aeruginosa* and 0.3 for Gram-positive bacteria (*S. aureus, E. faecalis* and *B. subtilis*), unless otherwise specified. To obtain the OD_{600} with NAC, a saline solution was supplemented with NAC at 10 mg/ml. To achieve a mixed suspension of 5 of these bacteria, 1/5 of the volume of each desired bacteria suspension was combined. Same procedure was followed for the selected fungi, *Candida albicans* (CECT 1394) and *Candida auris* (ATCC MYA-5001), but growing them in Yeast Peptone Dextrose (YPD) media (with or without agar in the base of the step) and adjusting the cell suspension OD_{600} to 0.5. In every case, 100 mm Petri dish plates with Miller's LB with agar were used for bacteria growth and antibacterial tests, while YPD with agar was used for yeast. All procedures were performed under biosafety level 2 laminar flow cabins and sterile conditions.

2.9. Single plate-serial dilution spotting (SP-SDS) methodology

Dried pristine and coated substrates (paper and cotton) were cut into pieces of 1.5 × 1.5 cm, introducing four of them (total area of 9 cm^2) in 10 ml glass vials, followed by 1 h of UV light for their sterilization. After obtaining the corresponding OD_{600} for all bacteria and fungi suspension, 120 μl were inoculated in the paper substrates and 300 μl in cotton. In the case of polypropylene, 4 discs of 0.9 cm (total area ≈ 2.5 cm^2) were inoculated with 30 μl. The volume selected in each case was the maximum capable of being retained by the material. For band-aids, 2 × 2 cm pieces were used and 150 μl for inoculation. After the desired incubation time of 30, 60, 180 min and 24 h, dilution −1 was obtained directly with the sample inside the glass vial in which it was incubated. Subsequently, it was sonicated for 5 min (Elmasonic S 30H) and the remaining serial dilutions (−2 to −5) were also created. Plates were seeded following the already described methodology for SP-SDS [26]. Then, the plates were incubated at 37 °C for 24 and 48 h for bacteria and fungi, respectively. Viable colony-forming units (CFU) were counted afterwards, with a total number of repetitions of N = 5 for each condition and N = 8 in the case of fungi. Results were represented with OriginPro version 9.8.0.200 software. Additionally, right after obtaining **PYRO-H** coated paper substrates, samples were kept in dry conditions and protected from light. The antibacterial activity of this coating was tested after being stored for 15, 30, 60, 120 and 180 days against *E. coli* and *S. aureus* after 3 h incubation.

2.10. Fluorescence viability test

To observe the cytotoxic effect of the coated substrate on the bacteria, the LIVE/DEAD™ BacLight™ L7012 Bacterial Viability Kit (Molecular Probes™, Invitrogen™) was used. This kit consists of two dyes, SYTO9 3.34 mM (which labels all bacteria populations) and propidium iodide (PI) 20 mM (which only penetrates when the membrane is damaged). Bacterial suspension was adjusted to OD_{600} 0.4 and 0.5 for *E. coli* and *S. aureus*, respectively. **PYRO-H**, **CAFF-H** coatings and pristine paper were inoculated with 120 μl of suspension and incubated for 3 h at 37 °C. Then, dilution −1 was obtained directly with the sample inside the vial and sonicated for 10 s. Afterwards, 500 μl of each sample were mixed with 1.5 μl of SYTO9 and 1.75 μl of PI and incubated at room temperature in darkness for 15 min. Finally, samples were observed with the Nikon ECLIPSE TE2000-E microscope, equipped with epifluorescence optics and a Hamamatsu ORCA-ER photographic camera. Pictures obtained for each dye in the same position were colored (Red-PI and Green-SYTO9) and merged with Image J software.

2.11. Microorganism visualization by SEM

Substrates containing bacteria were fixed with paraformaldehyde 2 % in a NaCl 0.9 % saline solution for 1 h. Subsequently, samples were dehydrated through an ethanol serial dilution series until 100 %. Then, samples were dried under cabin airflow, coated with a 5 nm layer of gold/palladium and finally observed by SEM. Bacteria SEM micrographs were colored using Adobe Photoshop CS6.

2.12. Generation of reactive oxygen species (ROS) test

ROS was measured with the fluorogenic kit MAK143. To measure the fluorescence generated by ROS from the coatings, black 96-well plates were selected. The antioxidant N-Acetyl-L-cysteine (NAC) was used to regulate the ROS generation of the coatings. Firstly, 180 μl of Master-Reaction-Mix (MRM) were mixed with 20 μl of MilliQ® water or NAC (achieving a final concentration of 1 or 10 mg/ml). Then, pristine, **PYRO-H** and **CAFF-H** coated paper substrates (6 × 0.5 cm) were introduced in the corresponding conditions: water (as a control), NAC 1 mg/ml or NAC 10 mg/ml. Finally, the fluorescence was measured every 20 min during 24 h, keeping a temperature of 25 °C (Varioskan™ LUX, Thermo Scientific™ and $\lambda_{excitation}$ = 490 nm/$\lambda_{emission}$ = 525 nm for excitation and emission wavelength, respectively). Three repetitions of each condition were performed, and the results were represented with OriginPro version 9.8.0.200 software.

2.13. Antioxidant protection effect in bacteria

Starting with a liquid culture of *E. coli*, two suspensions with an OD_{600} of 0.2 were obtained, one supplemented with NAC 10 mg/ml and the other not (control). Right after, **PYRO-H** and **CAFF-H** coated paper substrates were inoculated with each of the suspensions separately, incubated for 180 min at 37 °C and followed by SP-SDS evaluation to compare the CFU reduction. For each condition, 5 repetitions were performed.

2.14. Detection of different reactive oxygen species (ROS)

Three different fluorogenic kits were used to detect three specific reactive oxygen species: OxiVision™ 21,505 (KIT A), MitoROS™ OH580 16,055 (KIT B) and MitoROS™ 580 16,052 (KIT C), for hydrogen peroxide (H_2O_2), hydroxyl radicals ($^{\cdot}OH$) and superoxide anions ($^{\cdot}O_2^-$), respectively (AAT Bioquest, US, California). Samples of pristine, **PYRO-H** and **CAFF-H** coated paper of 6 × 0.5 cm were introduced in a black 96-well plate, while no substrate was counted as blank. The protocols described in each kit were followed unless otherwise specified. KIT A: after preparing the working-solution at 20 μM on 20 mM Hepes buffer, 200 μl were added to each condition; KIT B: after preparing the working-solution on the assay buffer as described, 200 μl were added to each condition; Kit C: after preparing the working-solution 2X in 20 mM Hepes buffer, 200 μl were added to each condition. All the samples and kits were prepared simultaneously and incubated for 30 min at room temperature and protected from light. Right after, KIT A was read at $\lambda_{excitation}$ = 490 nm/ $\lambda_{emission}$ = 525 nm, while KITs B and C at $\lambda_{excitation}$ = 510 nm/$\lambda_{emission}$ = 580 nm. At least 4 repetitions of each condition were performed, and the results were represented with OriginPro version 9.8.0.200 software.

2.15. Cell culture procedure

Fibroblasts (NIH/3T3, CRL-1658 ATCC) were cultured and maintained in 100 mm culture dishes (Falcon™ 353003, Fisher Scientific), using 10 ml of Dulbecco's modified Eagle's medium (DMEM), which was supplemented with 100 μg/ml streptomycin, 100 U/ml penicillin, and 10 % heat-inactivated fetal bovine serum (FBS) (Invitrogen). Cells were incubated at 37 °C in a saturating humidity atmosphere composed of 95 % air and 5 % CO_2 (Fisherbrand™ CO_2 Incubator Isotemp™). After achieving 80–90 % of confluence, cells were rinsed with phosphate-buffered saline (PBS, 100 mM pH 7.4) and incubated at 37 °C for 3 min with 0.05 % trypsin-EDTA until dissociated. Afterwards, DMEM with 10 % FBS was added to neutralize the trypsin and the resulting suspension was centrifuged at 200 g for 5 min. Finally, the pellet was resuspended in a complete medium and the density was adequately adjusted for the experiments. All procedures were performed in a biosafety level 2 laminar flow cabins in sterile conditions.

2.16. Cell viability assay

PrestoBlue™ cell viability kit (Invitrogen™) was used to evaluate the possible cytotoxic effects of the pristine and coated substrates in the NIH/3T3 cell line. Initially, a total of $5x10^4$ cells/well with 100 μl medium were seeded in a 96-well plate (Falcon™ 353072, Fisher Scientific) and incubated at 37 °C for 24 h. Then, the medium was changed to 100 μl of fresh one; cells without substrate were used as controls, while 5 mm^2 substrates (UV sterilized) were incorporated into each well, followed by incubation at 37 °C for 24 h. Afterwards, substrates and medium were removed and 10 μl of PrestoBlue™ cell viability kit were added to each well, incubated for 30 min following the manufacturer specifications and finally read (Victor3, PerkinElmer). In each plate, three replicates were done for each condition and a total of four repetitions (N = 4) were performed. Results were represented with OriginPro version 9.8.0.200 software.

2.17. Ex vivo antibacterial test

Fresh pig skin was extracted and stored in Krebs-Ringer HEPES-buffered solution at 4 °C until used (same day of extraction). After cutting pieces of 3 × 3 cm of skin, a hole of approximately 3 mm of depth was performed in the center of the sample using a 6 mm of diameter biopsy punch. Then, each piece was abundantly washed in sterile saline solution, placed in individual 6 cm sterile Petri dishes and 1 ml of saline solution added to the bottom. Subsequently, 50 μl of *E. coli* (OD 0.2) were inoculated in each hole, covered with pristine or **PYRO-H** coated band-aid and incubated for 24 h. Finally, SP-SDS counting was performed, with an N = 3 for each condition. All procedures were performed under biosafety level 2 laminar flow cabins and sterile conditions.

2.18. Statistical analysis

For SP-SDS logarithmic reduction test, the CFU number obtained for each plate/condition was transformed to a logarithm and represented as the mean ± standard deviation minus the control mean log(CFU) "$\overline{x}$". The detection limit was calculated following the next equation (A), where "CFU_{limit}" were the lowest countable colonies per plate 1, "N" number of repetitions (5 for bacteria and 8 for fungi), "d" dilution in which colonies were counted and "ml seeded" were 0.02 ml.

$$Detection\ limit\ =\ \log\left(\frac{CFU_{limit}}{N}\cdot\frac{0,1\ ml}{mL\ seeded}\cdot 10^{d+1}\right)\ -\overline{x}\ (A)$$

For the overall ROS generation test, the signal obtained for each time-measurement (every 20 min during 24 h) was represented as the mean ± standard deviation of the 3 repetitions of each condition. In the specific ROS generation test, the results obtained from each of the 3 kits were analysed separately, subtracting the mean of the blank from the mean achieved by the 4 repetitions of each condition (pristine, **PYRO-H** and **CAFF-H**) and represented as fold vs. the pristine paper mean signal. In the case of the NIH/3T3 cell viability test, results were normalized as a percentage of the control mean and represented as the mean ± standard deviation.

3. Results and discussion

3.1. Coatings on paper, properties and antibacterial activity

The bioinspired coatings were synthesized by combining different catechol derivatives: pyrocatechol (PYRO), caffeic acid (CAFF), pyrogallol (GALL), catechin (CAT), dopamine (DOPA) and 4-methylcatechol (4MET), with two amino-based ligands: hexamethylenediamine (HMDA, H) and tris(2-aminoethyl)amine (TRIS, T). The twelve developed coatings were respectively named: **PYRO-H**, **PYRO-T**, **CAFF-H**, **CAFF-T**, **GALL-H**, **GALL-T**, **CAT-H**, **CAT-T**, **DOPA-H**, **DOPA-T**, **4MET-H** and **4MET-T**. Briefly, the selected catechol-derivative and the amine-based ligand (Fig. 1**b**) were weighted separately and mixed in ultrapure water with different molarities (see Supporting Information, **Table S1**), in the presence of a paper substrate (see Supporting Information, **Fig. S1**). Interestingly, each catechol-derivative generated a coating with a specific colour, which slightly changed in base of the amine that was combined (Fig. 2**b**). The diverse colour palette achieved, obtaining yellow, orange, brown, green, beige, and pale rose coatings, enables this technology to be tailored and thus simplifies the implementation of the coatings based on the ultimate use**.** Furthermore, obtaining these coatings suggests that different di/tri-amines and catechol-derivatives could also be combined to create new ones with tuned characteristics.

3.1.1. Characterization

The polymerization and coating formation were confirmed by FT-IR, which clearly shows the presence of both HMDA (H) or TRIS (T) and catechol/quinonic species (see Supporting Information, **Fig. S2**). The broad band around 3240 cm^{-1} and its shoulder at higher wavenumbers around 3400 cm^{-1} could be attributed to the NH_2 and O–H vibrations from catechol and amine moieties, respectively. These observations confirmed the presence of both hydroxyl and free amino groups, which would have a relevant role in the retention and inactivation of pathogens. Interestingly, all spectra presented shoulders of intense bands around 1575 cm^{-1}, and between 1620 and 1710 cm^{-1}, which could be

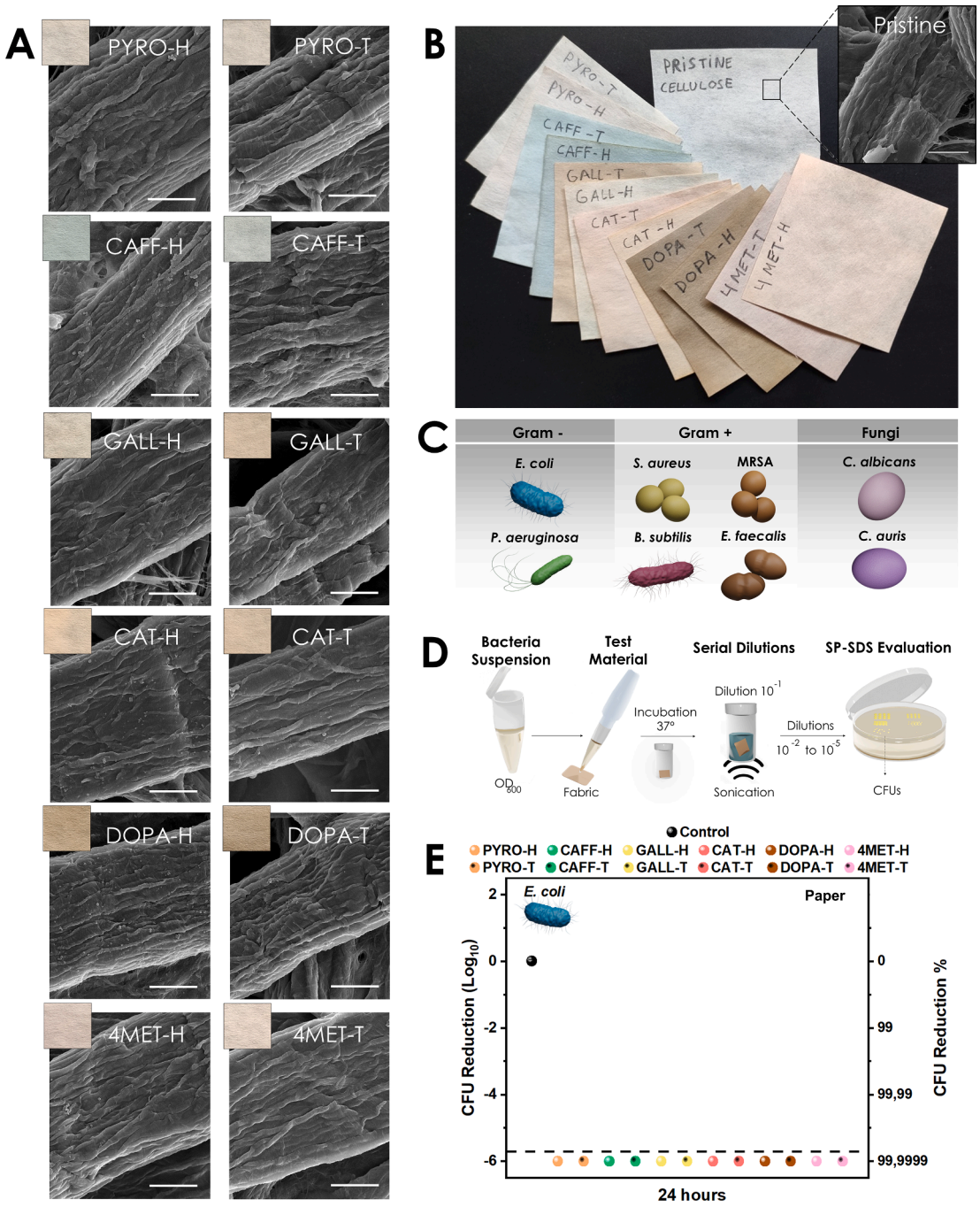

Fig. 2. The twelve catechol-based coatings with antibacterial properties. a) Scanning electron microscopy (SEM) micrographs of: PYRO-H, PYRO-T, CAFF-H, CAFF-T, GALL-H, GALL-T, CAT-H, CAT-T, DOPA-H, DOPA-T, 4MET-H and 4MET-T coatings in paper. b) Visual color comparison between a pristine substrate (paper) and different coatings obtained after permuting the catechol-derivatives and amines. Inset: SEM micrograph of pristine paper. c) All bacteria and fungi used in this work. d) Scheme of the single plate-serial dilution spotting (SP-SDS) methodology. e) Screening of the antibacterial properties of the twelve different coatings in paper after being inoculated with *E. coli* for 24 h. In all the cases, the colony-forming units (CFU) logarithmic reduction obtained was below the detection limit (dashed line). The SEM scale bars correspond to 5 μm.

attributed to C = O quinonic groups. The presence of hydroxyl and quinones groups is of special interest due to: i) offering interaction and strong adhesion with the substrates and ii) be further oxidized, thus producing ROS during the process. Finally, FT-IR allowed to confirm the presence of other functional groups. For example, when CAFF was used as a catechol-derivative, carboxylate groups ($–COO^-$) could be observed by identifying their characteristic bands at 1585 cm^{-1} and 1385 cm^{-1}. The surface exposure of those functional groups previously detected was further confirmed by using X-ray Photoelectron Spectroscopy (XPS) (see Supporting Information, **Fig. S3**). The coexisting catechol moieties with their oxidized quinone state were confirmed by the detection of C–OH and C = O signals at approximately 286 eV and 288 eV, respectively. Furthermore, the presence of aliphatic C–NH at approximately 399 eV would indicate the presence of unreacted amine tail ends. Interestingly, the aforementioned functional groups may be protonated/deprotonated under certain conditions of moisture and the presence of oxygen, endowing the bioinspired coatings with improved antimicrobial properties and electrostatic interactions at the bio-interface.

Scanning electron microscopy (SEM) images denoted a thin layer of catechol-amine coating homogeneously covering the fibers, with small

variations from one amino-based reagent to the other (Fig. 2**a**). Interestingly, the thicknesses of the coatings were homogeneous, showing values around 300 nm (see Supporting Information, Fig. S4**A** and **B**). Thanks to that, the fabrics retained the intrinsic mechanical properties of the substrate and their porous and permeable nature. This is especially relevant for those materials with applications in health environments that must accomplish specific permeability and breathability parameters (e.g., coats and face masks, among others). Further experiments were planned to validate the stability of our coatings. Following standard procedure, the coated materials underwent thorough washing with a continuous flow of distilled water and were subsequently dried under vacuum. This washing process was repeated until the resulting water became completely clear, indicating the removal of any unreacted materials and excess coating. Importantly, these washes did not alter the coating, providing evidence of its stability and strong adhesion to the underlying fiber substrates. Additionally, stability studies were performed by immersing the coatings in MilliQ® water for 60 days, with magnetic stirring. After this period, the coatings immersed in water were compared to those that remained dry by SEM, in order to find defects or signs of degradation. SEM images did not evidence any considerable variation in the overall aspect of all the coatings, neither the surface nor the amount of coating, suggesting that catechol-amine coatings possess excellent durability in water (see Supporting Information, **Fig. S5**).

Additionally, the surface charge of the twelve isolated coatings was measured to determine their potential electrostatic interactions (see Supporting Information, **Table S2**). The results revealed that most of the coatings exhibited a positive charge. Specifically, all the coatings synthesized with HMDA (except **CAFF-H**) showed positive surface charge values ranging from 11 to 37 mV, depending on the catechol derivative used. On the other hand, the **CAFF-H** coating had a nearly neutral charge (-0.3 ± 0.4 mV), which was likely due to the presence of deprotonated exposed carboxylic acid groups from the caffeic acid ligand. When HMDA was replaced with TRIS, the surface charge of all the coatings increased, getting values from 17 to 40 mV. This can be attributed to the fact that TRIS ligand has an extra amine group compared with HMDA. As discussed in the following sections, the positive surface charge of the coatings plays an essential role in their antimicrobial mechanisms and interactions with pathogens.

Finally, to demonstrate the biocompatibility, NIH/3T3 fibroblasts were exposed to all the catechol-based materials for 24 h. The results showed no significant differences in all conditions compared with the control (only cells) (see Supporting Information, **Fig. S6**), demonstrating cell viability higher than 90 % and thus corroborating their potential application in healthcare.

3.1.2. Antibacterial activity

The antibacterial activity of the twelve different coatings (as well as pristine paper for comparison purposes) against *E. coli* was tested. For this, we calculated the logarithmic reduction of the colony-forming units (CFUs) through the single plate-serial dilution spotting (SP-SDS) method using *E. coli* (Fig. 2**c,d**). Worth to mention, the antibacterial tests were performed under similar conditions found in real environments. After 24 h of incubation, no CFUs were detected in any of the coatings, revealing an antibacterial activity above 99.999 % (Fig. 2**e** and Supporting Information, **Table S3**). These results demonstrated the high antibacterial effectivity of the synthesized coatings against a resistant and widespread bacteria strain, suggesting a common antibacterial pathway for the developed phenolic-based coatings.

3.2. Antimicrobial range of action

To validate our approach beyond *E. coli*, the antimicrobial properties were studied over a broader range of pathogens. Given the experimental challenge of carrying out these experiments on the twelve substrates, we focused on **PYRO-H** and **CAFF-H** as representative coatings. The selection was based on: i) chemical composition (different exposed functional groups), ii) cost-production and iii) optimum coating homogeneity.

3.2.1. Determination of the minimum contact-killing time

Prior to the study, the minimum effective antibacterial activity of **PYRO-H** and **CAFF-H** was tested against Gram-negative (*E. coli*) and Gram-positive (*S. aureus*) bacteria strains in a time-lapse of 30, 60 and 180 min (Fig. 3**a**). After 30 min, a CFU log reduction of approximately −1 was observed, without significant differences between both bacteria and coatings. Interestingly, the antibacterial effect increased with time, reaching its maximum activity after 180 min, when the CFUs decreased dramatically and reached the detection limit in almost all the conditions, especially for the *E. coli* strain (no effect was found for the control sample, see Supporting Information, **Fig. S7**). Worth to mention, the **CAFF-H** coating was less effective with *S. aureus* in comparison to **PYRO-H**, most probably due to electrostatic repulsion between deprotonated carboxylic acids exposed on the coating surface and the negative charges surrounding bacteria. Overall, 180 min was selected as the optimal incubation period.

3.2.2. Spectrum of antimicrobial activity

The antibacterial properties of **PYRO-H** and **CAFF-H** coatings in paper with four additional bacteria (*P. aeruginosa,* MRSA, *E. faecalis* and *B. subtilis*, Fig. 3**b**) and two fungi (*C. albicans* and *C. auris*, Fig. 3**c**) were tested at 180 min and 24 h, respectively. As can be seen in Fig. 3**b, PYRO-H** achieved a considerably higher CFU reduction than **CAFF-H** with Gram-positive bacteria, whereas no significant differences were found in the Gram-negative bacteria. As previously discussed, these differences could be attributed to the different electrostatic interactions established between both coatings and the bacteria plasma membrane. Additionally, the antibacterial activity of **PYRO-H** or **CAFF-H** in contact with *E. coli* and *S. aureus* after 180 min was confirmed by live/dead fluorescent staining. More dead (red) than alive (green) cells were observed by fluorescence in the coated substrates, especially in *E. coli*, than in the pristine substrate (see Supporting Information, **Fig. S8**).

Similar behaviour was found for fungi, where both coatings exhibited antimicrobial activity (Fig. 3**c**). While **PYRO-H** was close to the detection limit (for *C. albicans*), **CAFF-H** easily overpassed it in both yeasts (Fig. 3**c** and Supporting Information, **Fig. S9** and **Table S3**). It is well known that the yeast form of *C. albicans* presents other non-specific mechanisms in addition to electrostatic interactions that allows for its spread. These mechanisms primarily involve physical interactions at the molecular level, allowing the fungus and similar pathogens to adapt to environmental changes, enhancing its adhesion to different surfaces [27]. Besides, it has been recently reported that caffeic acid (precursor of **CAFF-H**) targets inhibition of key enzymes involved in the survival of fungi [28]. All this could explain the higher antifungal efficiency observed in the **CAFF-H** coating compared to **PYRO-H**. A visual comparison of the antifungal activity with the substrate can be found in Supporting Information, **Fig. S10**.

3.3. Antimicrobial mechanism

The remarkable antimicrobial effectiveness previously observed may arise from a complex mechanism that is activated upon direct contact of pathogens with the coated surfaces, favoured by the adhesion properties of phenol-based coatings and the electrostatic interactions. The first killing mechanism is the production of ROS. For this reason, the ability to generate ROS by **PYRO-H** and **CAFF-H** coated paper in wet environments was studied. The ROS production capacity of the coatings was monitored for 24 h. Interestingly, the results showed how both coatings generated sustained ROS production over time (Fig. 4**a**). Moreover, **PYRO-H** induced a higher signal than **CAFF-H**, which could explain why the first one achieved better overall results in the antimicrobial assays. Additionally, to corroborate the ROS generation by the coatings and its modulation, N-Acetyl-L-Cysteine (NAC) at concentrations of 1 and 10 mg/ml was added. With the presence of the antioxidant, a decrease in

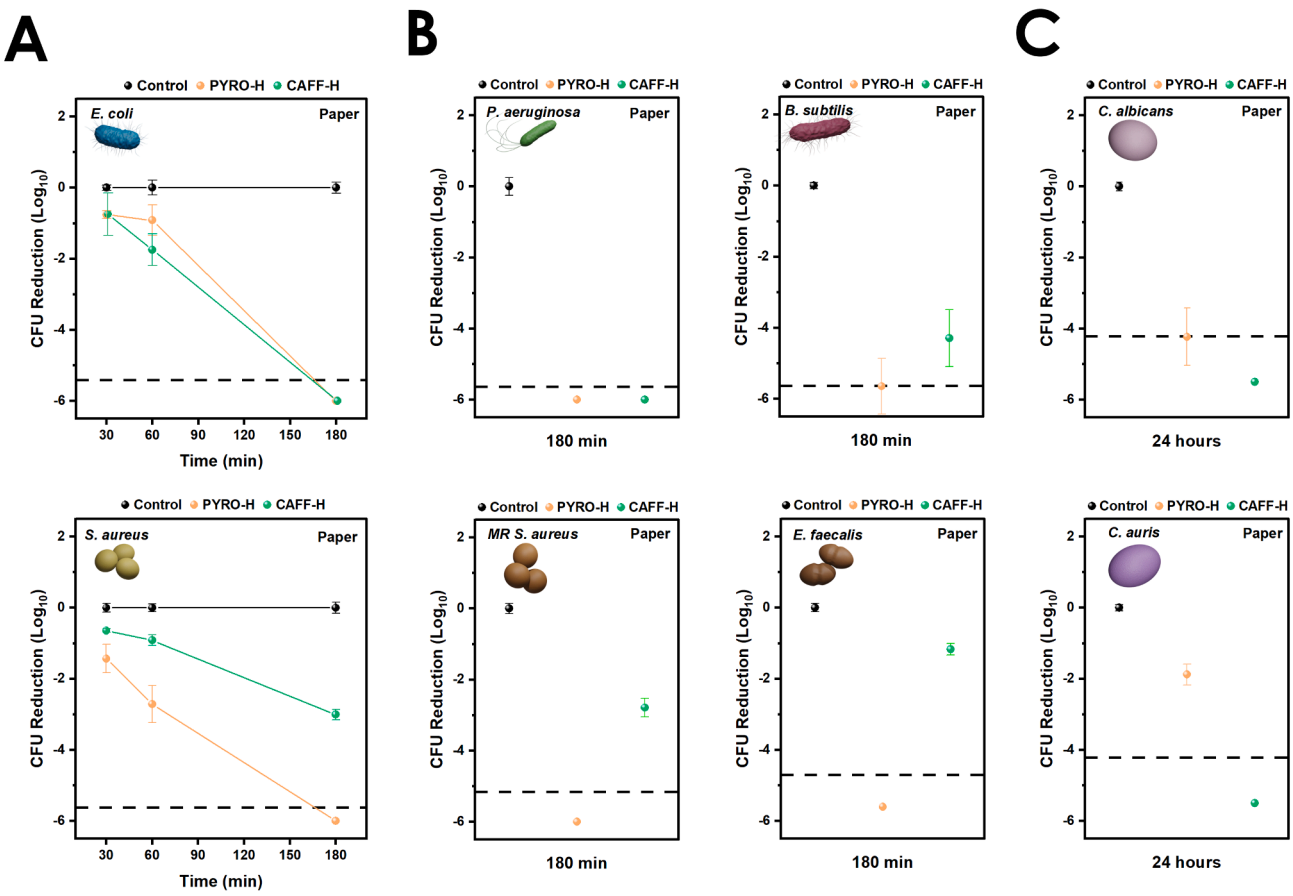

Fig. 3. Broad antimicrobial spectrum of the two selected catechol-based coatings. a) CFU logarithmic reduction, in base of exposure time, on paper substrates, with PYRO-H or CAFF-H coatings against *E. coli* and *S. aureus*. CFU logarithmic reduction in coated paper with PYRO-H and CAFF-H after: b) 3 h of incubation against four bacteria (*P. aeruginosa,* MRSA, *B. subtilis and E. faecalis*) and c) 24 h against two fungi (*C. albicans* and *C. auris*). The dashed line represents the detection limit.

the signal of both coatings was observed (Fig. 4**a**), turning to almost zero in the case of 10 mg/ml (see Supporting Information, **Fig. S11**). These results demonstrated the ROS activity of the coatings and their continuous release.

Furthermore, to compare the antibacterial properties of these materials in the presence or absence of an antioxidant, two suspensions of *E. coli,* with and without supplementation of 10 mg/ml of NAC, were tested for 3 h in uncoated and **PYRO-H** and **CAFF-H** coated paper substrates. Despite the slight toxic effect of NAC observed in the pristine paper, the resulting plates showed a clear decrease in the antibacterial activity of both coatings (slightly more in **CAFF-H**) when this ROS-scavenger was present (see Supporting Information, **Fig. S12** and **Table S4**). These results confirmed the suggested mechanism based on sustained ROS production.

Going a step further, the production of specific reactive oxygen species was also assessed in **PYRO-H** and **CAFF-H** coated paper (see Supporting Information, **Fig. S13**). When compared against the uncoated substrate, both coatings generated hydrogen peroxide, especially **PYRO-H**. However, only **CAFF-H** showed remarkable signs of hydroxyl radicals and superoxide anion production (see Supporting Information, **Fig. S13**). Worth to mention, ROS species such as H_2O_2 or $^{\cdot}OH$ lack potent disinfectant effects or have a short half-life [21]. For this reason, the outstanding antimicrobial effectiveness suggests other interactions. In this sense, a second mechanism could be induced due to the presence of protic amine groups on the surface, which endow the coatings with positive charges (see Supporting Information, **Table S2**) that could interact with the negatively charged cell wall of the bacteria [14].

The electrostatic attractive interactions play a crucial role in promoting close contact between microorganisms and the surface of the coating. This process is essential to make more effective both adhesion and ROS effect. The bioinspired coatings described in this study exhibited a multi-pathway antimicrobial activity, which is further enhanced by the adhesion properties provided by catechol groups (Fig. 4**b**). The mechanisms and interactions previously described result in irreversible damage to the pathogens based on: i) physical lysis, ii) charge disruption and iii) exudation of cell contents.

To validate this multi-step mechanism, the six bacteria and the two fungi tested were visualized by SEM after interacting for 180 min and 24 h, respectively, with **PYRO-H** and **CAFF-H** coatings and the pristine paper (Fig. 4**c**). In all cases, the direct contact between the coating and the pathogens led to a severely damaged plasma membrane, showing an irregular and deflated shape, which compromised their viability. The coating antimicrobial effect was evident when the pathogens in contact with uncoated paper were compared, showing that bacteria and fungi had normal morphology and were visually viable (Fig. 4**c**). Similar results were observed after seeding a bacterial cocktail. In this case, a mixture of *E. coli, P. aeruginosa*, *S. aureus*, *E. faecalis* and *B. subtilis* were inoculated against **PYRO-H** and **CAFF-H** coated papers for 180 min. Interestingly, SEM micrographs showed bacteria-damaged morphology simultaneously for all tested strains (Fig. 4**d**). Besides, no CFUs were observed in the SP-SDS plates in the case of **PYRO-H** (see Supporting Information, **Fig. S14**). Overall, these results demonstrated the broad antimicrobial range of action of the developed coatings, even when mixing different strains in the same coating.

Additionally, the specific antibacterial activity of **PYRO-H** was studied and compared at different time intervals of 0, 15, 30, 60, 120 and 180 days. Samples were stored in dark and dry conditions since their fabrication until they were used. CFU reduction was assessed with *E. coli*

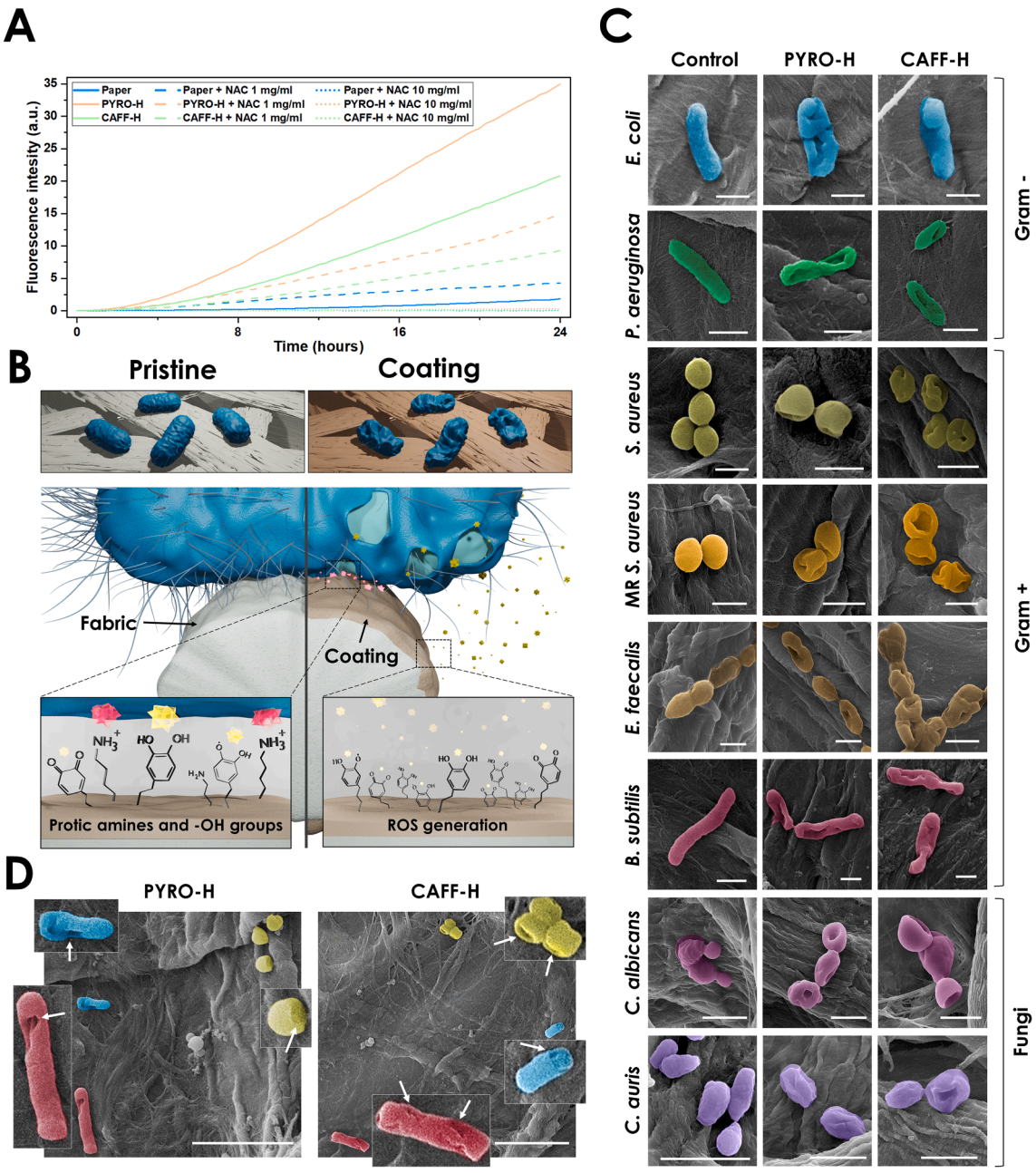

Fig. 4. Antimicrobial mechanisms of the coatings compromising the integrity of pathogens a) Reactive oxygen species (ROS) generation, comparing the signal obtained by pristine, PYRO-H and CAFF-H coated paper in presence or absence of N-Acetyl-L-Cysteine (NAC) (1 and 10 mg/ml) for 24 h. b) Scheme of the proposed antimicrobial mechanisms involved in microbial wall damage observed: i) retention by catechol groups, ii) interaction of protic amines, and iii) ROS generated by the active oxidation of exposed functional groups from the coatings. c) Coloured SEM images of the eight different microorganisms (Gram-negative: *E. coli* and *P. aeruginosa*, Gram-positive: *S. aureus*, methicillin-resistant *S. aureus* (MRSA), *E. faecalis*, *B. subtilis*, Fungi: *C. albicans* and *C. auris*) in pristine paper (left), PYRO-H (centre) and CAFF-H (right) coatings. Pathogens in the control substrate showed a stable morphology and were visually viable. Those microorganisms in contact with coatings, presented severely damaged membranes and irregular shapes. The scale bars correspond to 1 μm for bacteria (Gram-negative and Gram-positive) and 5 μm for Fungi. d) Inoculated bacteria cocktail (*E. coli*, *P. aeruginosa*, *S. aureus*, *E. faecalis* and *B. subtilis*), showing their non-viability in PYRO-H and CAFF-H coatings in paper.

and *S. aureus*, following the previous protocols for 180 min of incubation. After comparing the results of the time course, no changes were observed in the antibacterial activity for both bacteria, at least after 2 months. Interestingly, a decrease in activity was observed after 4 months. Nevertheless, still excellent results were obtained, with reductions in *E. coli* and *S. aureus* higher than 99.9 % and 99 %, respectively (see Supporting Information, **Table S4**). Finally, after 6 months, approximately 90 % reduction could still be achieved in both bacteria (see Supporting Information, **Fig. S15**). These results demonstrated the stability and long-lasting ROS generation activity of the developed coatings.

3.4. Antibacterial activity on different substrates

3.4.1. Coating universality

The coating ability to be used on different substrates was validated by applying both **PYRO-H** and **CAFF-H** to cotton and polypropylene obtained from a lab coat and surgical mask, respectively (Supporting

Information **Fig. S16**). Like paper, the coatings were homogenously distributed, covering the fibers without clogging the pores and retaining their intrinsic permeability properties (Fig. 5**a**), with some rugosities of no relevance (see Supporting Information, **Fig. S17**). Overall, these results corroborate the fine-tuned control of the coatings independently on the target substrate, without any previous functionalization. Moreover, and what is even more relevant for proper performance, the presence of the coating modified the wettability of the substrates. For instance, the hydrophobic nature of polypropylene becomes hydrophilic and adsorbs water upon coating. This was corroborated by measuring the contact angle of the pristine and coated polypropylene, obtaining 126° and 0°, respectively (see Supporting Information, **Fig. S18**).

Pristine polypropylene has antifouling properties mainly due to its hydrophobic nature, which repels bacteria but still allows them to spread to other surfaces. The modification of polypropylene through the bioinspired coatings enables the formation of a hydrophilic substrate, avoiding the antifouling effect and allowing direct contact with bacteria. Therefore, these bacteria can be retained and eliminated through the mechanisms previously described. The presence of a hydrophilic environment is crucial as it promotes interactions between bacteria and surfaces, thereby enhancing the antibacterial effect at the bio-interface [29].

3.4.2. *Antibacterial activity*

The antimicrobial action of the **PYRO-H** and **CAFF-H** coatings on cotton and polypropylene against *E. coli* and *S. aureus* at 180 min was also tested. A visual comparison of the antibacterial properties in paper and cotton for both bacteria is found in Supporting Information, **Fig. S19**. In the case of polypropylene, strong antibacterial activity was observed for both coatings against both bacteria **(**Fig. 5**b)**. However, a lower antibacterial effect was observed for cotton coated with **CAFF-H**, especially with *E. coli* (Fig. 5**b**). These differences could be tentatively attributed to the intrinsic properties of the material in terms of permeability, fiber content, morphological structure and how it fine-tunes the interactions with bacteria (see Supporting Information, **Fig. S20**). These properties could influence the interactions with bacteria, resulting in lower or higher antibacterial activity efficiency. Interestingly, the universal application of the developed coatings allows for overcoming these differences by selecting and adapting the preferred substrate based on the final application.

3.5. *Proof-of-concept case: In vitro and ex vivo validation of commercial band-aids*

As a proof-of-concept for the evaluation of the developed coatings, both **PYRO-H** and **CAFF-H** coatings were performed on commercial band-aids (composite material) (Fig. 6**a** and Supporting Information **Fig. S21**). The coatings were performed for 18 h ensuring a complete and homogenous covering around the fibers composing the band-aids (Fig. 6**b** and Supporting Information **Fig. S21**). Once the coating was successful, the antibacterial properties of the resulting coated substrates were tested against *E. coli* and *S. aureus* for 24 h. When *S. aureus* was analysed, a CFU reduction of at least 99.99 % was observed for both coatings (detection limit). Interestingly, slightly lower results were obtained with *E. coli* for both **PYRO-H** and **CAFF-H** coatings, being approximately 99.9 % and 99 %, respectively (Fig. 6**c** and Supporting Information **Fig. S22**).

For further validation, the antibacterial properties were tested in a more realistic environment using *ex vivo* tissue. An infection scenario was mimicked using fresh pieces of pig skin, establishing a simulation of a wound model by performing a hole in the skin and subsequent inoculation of *E. coli* (Fig. 6**d**). The mimicked infected wound was covered with pristine or coated band-aids. In this case, **PYRO-H** was selected as a candidate due to its overall superior antimicrobial properties previously discussed. Remarkably, after 24 h of incubation, **PYRO-H** achieved an outstanding 90 % CFU reduction present in the infected *ex vivo* wound

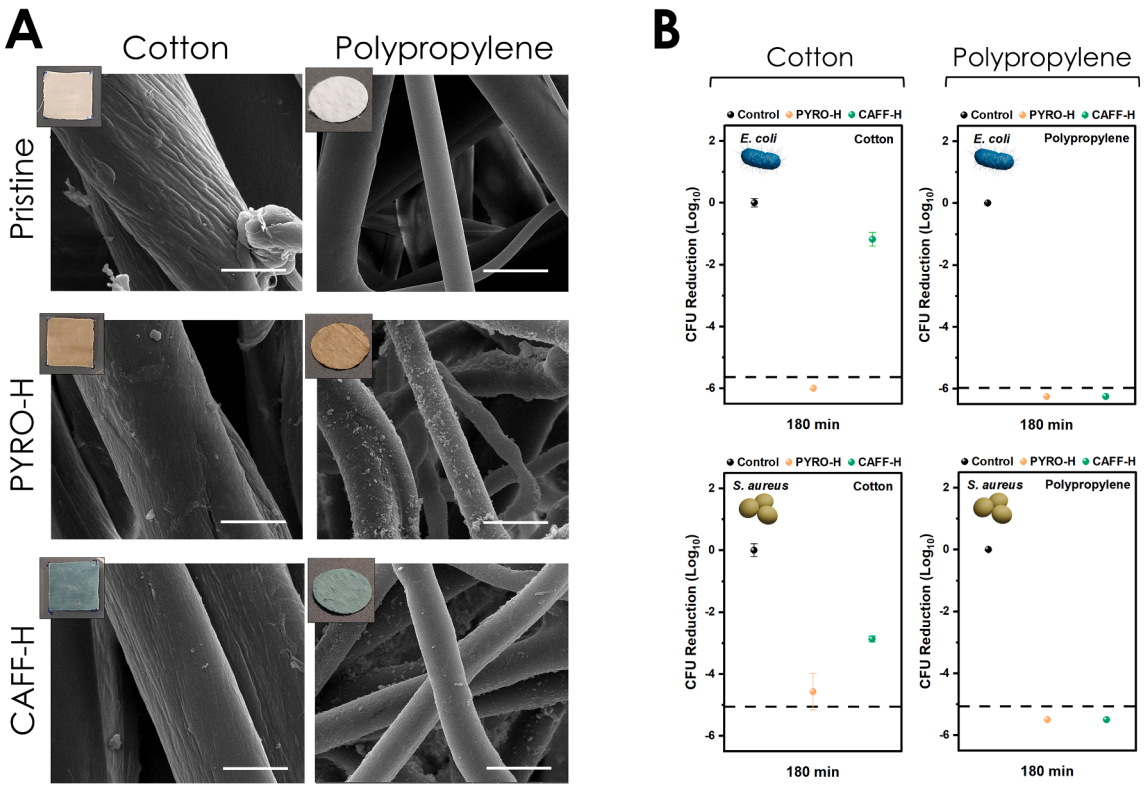

Fig. 5. Robustness of the antimicrobial properties. a) SEM micrographs of the selected PYRO-H and CAFF-H coatings in cotton (left) and polypropylene (right) substrates. The SEM scale bars correspond to 5 μm. b) CFU logarithmic reduction of *E. coli* and *S. aureus* in coated cotton and polypropylene with PYRO-H and CAFF-H after 3 h of incubation. The dashed line represents the detection limit.

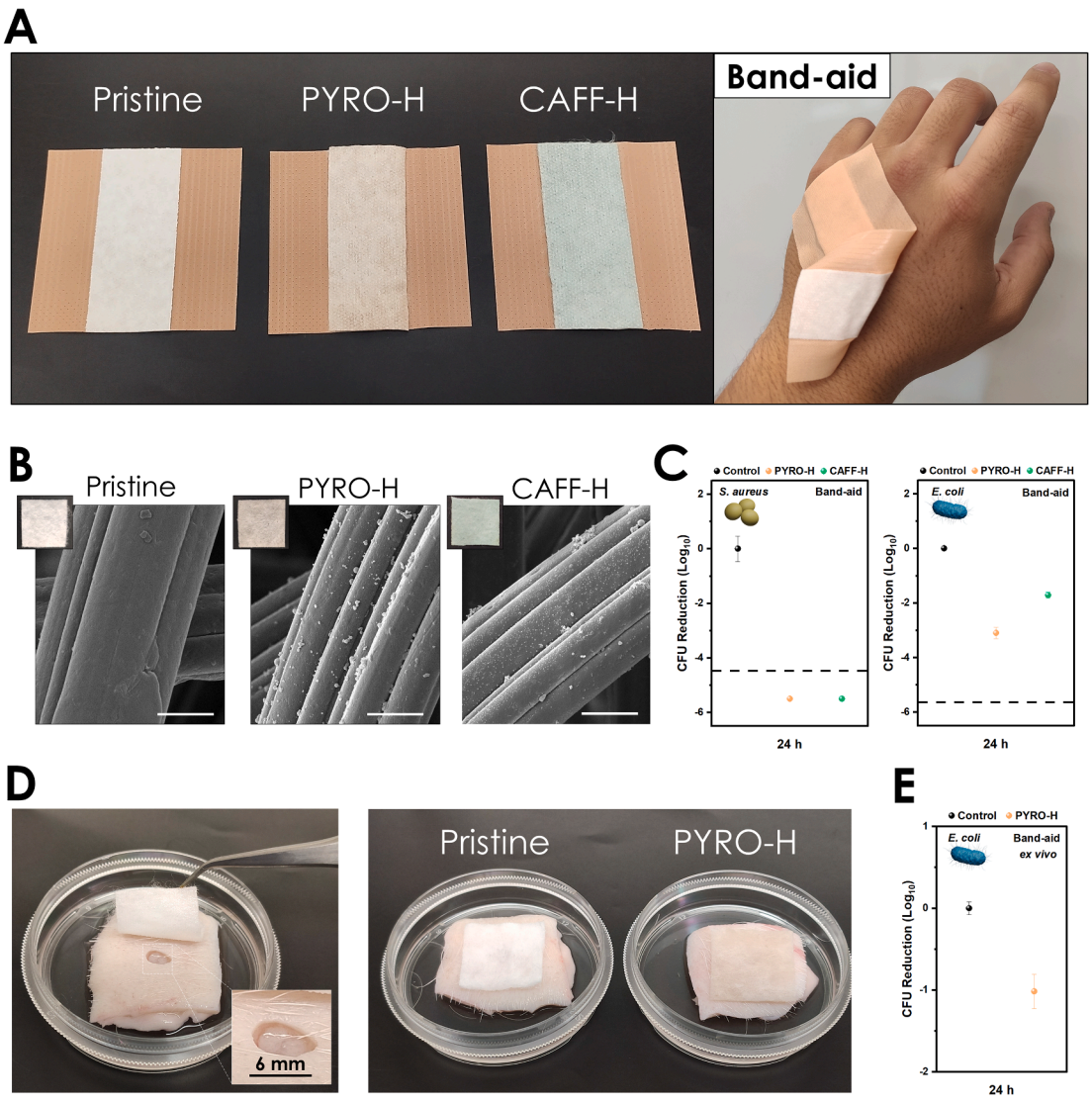

Fig. 6. Antibacterial properties in commercial band-aids. a) Visual comparison between pristine, PYRO-H and CAFF-H coated band-aid. b) SEM pictures of pristine and coated band-aid fibers. The SEM scale bars corresponds to 5 μm. c) CFU logarithmic reduction of both coatings against *S. aureus* and *E. coli* after 24 h incubation (dash line represents the detection limit). d) *Ex vivo* assays performed in pig skin. e) CFU reduction achieved by PYRO-H against *E. coli* after 24 h over the inoculated tissue.

(Fig. 6**e** and Supporting Information **Fig. S22c)**. These results suggested the excellent ability of the coatings for their potential application against bacteria spread, avoiding infection progression.

4. Conclusions

Catechol-amine-based coatings universally perform on different substrates of relevance in healthcare environments: paper, cotton, surgical mask middle layer and commercial band-aids. The resulting coated materials were able to completely eradicate several microorganisms, being especially relevant different bacteria (*E. coli*, *P. aeruginosa*, *S. aureus*, MRSA and *E. faecalis*) and fungi (*C. albicans* and *C. auris*), which are considered global health threats due to their AMR. Moreover, its efficient application was demonstrated in wet atmospheres, like those found in healthcare environments, where respiratory droplets and/or other biofluids are present, thus reducing the risk of indirect contact transmission. Such antimicrobial activity was attributed to a direct contact killing process, where the pathogen is initially attached to the coating by catechol molecules and other polyphenol derivatives. Then, a multi-pathway antibacterial effect is activated, mainly focused on: i) a sustained generation of biosafety levels of ROS and ii) electrostatic interactions with protic amino groups exposed to the surface. These antibacterial mechanisms induced a fast (180 min for bacteria and 24 h for fungi) and efficient (more than 99 %) response against pathogens, causing irreversible damage.

Our developed coatings follow a simple one-step and scalable synthesis under mild conditions, using affordable materials and green chemistry-based methodologies. Besides, the polyphenolic nature of their composition and the absence of additional external antimicrobial agents enhance the simplicity of the bioinspired coatings and avoid the induction of AMR and its cytotoxic effects on host cells and the environment. Worth to mention, different parameters such as colour, thickness and adhesion were fine-tuned, thus offering an adaptable solution for the different demands of the final material application. All-in-all, the designed bioinspired coatings have demonstrated a huge potential for further translation into clinics, as they represent a feasible alternative to existing antimicrobial materials.

CRediT authorship contribution statement

Jose Bolaños-Cardet: Data curation, Investigation, Methodology, Writing – review & editing, Validation, Writing – original draft. **Daniel Ruiz-Molina:** Funding acquisition, Writing – review & editing. **Victor J. Yuste:** Funding acquisition, Resources, Supervision, Writing – review & editing. **Salvio Suárez-García:** Conceptualization, Formal analysis, Investigation, Methodology, Project administration, Supervision, Writing – original draft, Writing – review & editing.

Declaration of competing interest

The authors declare that they have no known competing financial interests or personal relationships that could have appeared to influence the work reported in this paper.

Data availability

Data will be made available on request.

Acknowledgments

This work was supported by grant PID2021-127983OB-C21 financed by MCIN/ AEI/10.13039/501100011033/ and ERDF "A way to make Europe", and SAF2017-83206-R funded by MCIN/Government of Spain and ERDF "A way to make Europe". The ICN2 is funded by the CERCA programme/Generalitat de Catalunya. The ICN2 is supported by the Severo Ochoa Centres of Excellence programme, Grant CEX2021-001214-S, funded by MCIN/AEI/10.13039.501100011033. JB-C is recipient of a "Personal Investigador en Formació" fellow (2020/D/LE/CC/3) from Universitat Autònoma de Barcelona.

Appendix A. Supplementary data

Supplementary data to this article can be found online at https://doi.org/10.1016/j.cej.2024.148674.

References

[1] Bracing for Superbugs, United Nations Environmnet Programme, **2023**, ISBN:978-92-807-4006-6.

[2] Antimicrobial resistance, World Health Organization. https://www.who.int/news-room/fact-sheets/detail/antimicrobial-resistance , 2021 (accessed: 30 August 2023).

[3] Jim O'Neill, Tackling drug-resistant infections globally: final report and recommendations the review on antimicrobial resistance, **2016**. https://amr-review.org/sites/default/files/160518_Final%20paper_with%20cover.pdf.

[4] M. Cloutier, D. Mantovani, F. Rosei, Antibacterial coatings: challenges, perspectives, and opportunities, Trends Biotechnol. 33 (2015) 637–652, https://doi.org/10.1016/j.tibtech.2015.09.002.

[5] L. Yang, C. Wang, L. Li, F. Zhu, X. Ren, Q. Huang, Y. Cheng, Y. Li, Adv. Funct. Mater. 32 (2021) 2108749, https://doi.org/10.1002/adfm.202108749.

[6] a) H.G. Menge, N.D. Huynh, K. Choi, C. Cho, D. Choi, Y.T. Park, Body-patchable, antimicrobial, encodable TENGs with ultrathin, free-standing, translucent chitosan/alginate/silver nanocomposite multilayers, Adv. Funct. Mater. 33 (2023) 2210571, https://doi.org/10.1002/adfm.202210571;
b) M. Chao, S. Wang, J.-H. Hu, B.-H. Lu, Q.-Y. Wang, S.-Q. Zhang, Silver cluster-porphyrin-assembled materials as advanced bioprotective materials for combating superbacteria, Adv. Sci. 9 (2022) 2103721, https://doi.org/10.1002/advs.202103721;
c) K.Y. Kwon, S. Cheeseman, A. Frias-De-Diego, H. Hong, J. Yang, W. Jung, H. Yin, B.J. Murdoch, F. Scholle, N. Crook, E. Crisci, M.D. Dickey, V.K. Truong, T. Kim, A liquid metal mediated metallic coating for antimicrobial and antiviral fabrics, Adv. Mater. 33 (2021) 2104298, https://doi.org/10.1002/adma.202104298.

[7] a) G.V. Vimbela, S.M. Ngo, C. Fraze, L. Yang, D.A. Stout, Antibacterial properties and toxicity from metallic nanomaterials, Int. J. Nanomed. 12 (2017) 3941–3965, https://doi.org/10.2147/ijn.s134526;
b) S. Szunerits, R. Boukherroub, Antibacterial activity of graphene-based materials, J. Mater. Chem. B 4 (2016) 6892–6912, https://doi.org/10.1039/C6TB01647B.

[8] a) Y.-Q. Zhao, Z. Xiu, R. Wu, L. Zhang, X. Ding, N. Zhao, S. Duan, F.-J. Xu, A near-infrared-responsive quaternary ammonium/gold nanorod hybrid coating with enhanced antibacterial properties, Adv. Nanobiomed Res. 2 (2022) 2200111, https://doi.org/10.1002/anbr.202200111;
b) E.A. Saverina, N.A. Frolov, O.A. Kamanina, V.A. Arylapov, A.N. Vereshchagin, V.P. Ananikov, From antibacterial to antibiofilm targeting: an emerging paradigm shift in the development of quaternary ammonium compounds (QACs), ACS Infect. Dis. 9 (9) (2023) 394–422, https://doi.org/10.1021/acsinfecdis.2c00469;
c) M. Sorci, T.D. Fink, V. Sharma, S. Singh, R. Chen, B.L. Arduini, K. Dovidenko, C. L. Heldt, E.F. Palermo, R.H. Zha, Virucidal N95 respirator face masks via ultrathin surface-grafted quaternary ammonium polymer coatings, ACS Appl. Mater. Interfaces B 14 (2022) 25135–25146, https://doi.org/10.1021/acsami.2c04165.

[9] a) D. Han, X. Liu, S. Wu, Metal organic framework-based antibacterial agents and their underlying mechanisms, Chem. Soc. Rev. 51 (2022) 7138–7169, https://doi.org/10.1039/D2CS00460G;
b) L. Yan, A. Gopal, S. Kashif, P. Hazelton, M. Lan, W. Zhang, X. Chen, Metal organic frameworks for antibacterial applications, Chem. Eng. J. 435 (2022) 134975, https://doi.org/10.1016/j.cej.2022.134975.

[10] a) H. Kong, G. Yang, P. He, D. Zhu, X. Luan, Y. Xu, R. Mu, G. Wei, Self-assembly of bioinspired peptides for biomimetic synthesis of advanced peptide-based nanomaterials: a mini-review, Nano Futures 7 (2023) 012001, https://doi.org/10.1088/2399-1984/acafbe;
b) N.D.T. Tram, J. Xu, D. Mukherjee, A.E. Obanel, V. Mayandi, V. Selvarajan, X. Zhu, J. Teo, V.A. Barathi, R. Laksminarayanan, P.L.R. Ee, Bacteria-responsive self-assembly of antimicrobial peptide nanonets for trap-and-kill of antibiotic-resistant strains, Adv. Func. Mater. 33 (2023) 2210858, https://doi.org/10.1002/adfm.202210858;
c) G. Li, Z. Lai, A. Shan, Advances of antimicrobial peptide-based biomaterials for the treatment of bacterial infections, Adv. Sci. 10 (2023) 2206602, https://doi.org/10.1002/advs.202206602;
d) V. Milosavljevic, L. Kosaristanova, K. Dolezelikova, V. Adam, M. Pumera, Microrobots with antimicrobial peptide nanoarchitectonics for the eradication of antibiotic-resistant biofilms, Adv. Funct. Mater. 32 (2022) 2111935, https://doi.org/10.1002/adfm.202112935;
e) A. Rai, R. Ferrão, T. Patricio, P. Parreira, E. Anes, C. Tonda-Turo, M.C. L. Martins, N. Alves, L. Ferreira, Antimicrobial peptide-based materials: opportunities and challenges, J. Mater. Chem. B 10 (2022) 2384–2429, https://doi.org/10.1039/D1TB02617H;
f) Y. Huo, J. Hu, Y. Yin, P. Liu, K. Cai, W. Ji, Self-Assembling Peptide-Based Functional Biomaterials Chembiochem. 24 (2023) e202200582, https://doi.org/10.1002/cbic.202200582.

[11] M. Maas, J. Wehling, Carbon Nanomaterials for Antibacterial Applications, in: Eds: L. Treccani, F. Meder (Eds.), Surface-Functionalized Ceramics: For Biotechnological and Environmental Applications, Wiley-VCH, Weinheim, Germany, 2023, pp.337–368. https://doi.org/10.1002/9783527698042.ch9.

[12] H. Luo, X.-Q. Yin, P.-F. Tan, Z.-P. Gu, Z.-M. Liu, L. Tan, Polymeric antibacterial materials: design, platforms and applications, J. Mater. Chem. B 9 (2021) 2802–2815, https://doi.org/10.1039/D1TB00109D.

[13] a) J. Saiz-Poseu, J. Mancebo-Aracil, F. Nador, F. Busqué, D. Ruiz-Molina, The chemistry behind catechol-based adhesion, Angew. Chem., Int. Ed. 58 (2019) 696–714, https://doi.org/10.1002/anie.201801063;
b) J. Sedó, J. Saiz-Poseu, F. Busqué, D. Ruiz-Molina, Catechol-based biomimetic functional materials, Adv. Mater. 25 (2012) 653–701, https://doi.org/10.1002/adma.201202343;
c) J. Guo, T. Suma, J.J. Richardson, H. Ejima, Modular assembly of biomaterials using polyphenols as building blocks, Biomater. Sci. Eng. 5 (2019) 5578–5596, https://doi.org/10.1021/acsbiomaterials.8b01507.

[14] a) Y. Fu, L. Yang, J. Zhang, J. Hu, G. Duan, X. Liu, Y. Li, Z. Gu, Polydopamine antibacterial materials, Mater. Horiz. 8 (2021) 1618–1633, https://doi.org/10.1039/D0MH01985B;
b) I. Singh, G. Dhawan, S. Gupta, P. Kumar, Recent advances in a polydopamine-mediated antimicrobial adhesion system, Front. Microbiol. 11 (2021) 607099, https://doi.org/10.3389/fmicb.2020.607099.

[15] a) F. Centurion, R. Namivandi-Zangeneh, N. Flores, M. Tajik, S. Merhebi, R. Abbasi, M. Mayyas, F.M. Allioux, J. Tang, W.A. Donald, C. Boyer, M.D. Dickey, K. Kalantar-Zadeh, A. Rahim, Liquid metal-triggered assembly of phenolic nanocoatings with antioxidant and antibacterial properties, ACS Appl. Nano Mater. 4 (2021) 2987–2998, https://doi.org/10.1021/acsanm.1c00125;
b) Z. Tian, G. Wu, M. Libby, K. Wu, K.J. Jong, Y.J. Kim, Synthesis of biologically derived poly(pyrogallol) nanofibers for antibacterial applications, J. Mater. Chem. B 11 (2023) 3356–3363, https://doi.org/10.1039/D3TB00312D;
c) H. Fu, J. Yang, Z. Shen, Y. Zhang, S. Kuang, L. Li, Z. Lin, X. Shi, Antibacterial, wet adhesive, and healing-promoting nanosheets for the treatment of oral ulcers, Biomater. Sci. 11 (2023) 3214–3226, https://doi.org/10.1039/D2BM02063G;
d) G. Pan, F. Li, S. He, W. Li, Q. Wu, J. He, R. Ruan, Z. Xiao, J. Zhang, H. Yang, Mussel- and barnacle cement proteins-inspired dual-bionic bioadhesive with repeatable wet-tissue adhesion, multimodal self-healing, and antibacterial capability for nonpressing hemostasis and promoted wound healing, Adv. Funct. Mater. 32 (2022) 2200908, https://doi.org/10.1002/adfm.202200908;
e) P. Liu, Y. Wu, B. Mehrjou, K. Tang, G. Wang, P.K. Chu, Versatile phenol-incorporated nanoframes for in situ antibacterial activity based on oxidative and physical damages, Adv. Funct. Mater. 32 (2022) 2110635, https://doi.org/10.1002/adfm.202110635.

[16] a) M. Dryden, Reactive oxygen species: a novel antimicrobial, Int. J. Antimicrob. Agents 51 (2018) 299–303, https://doi.org/10.1016/j.ijantimicag.2017.08.029;
b) P.-L. Lam, R.-S.-M. Wong, K.-H. Lam, L.-K. Hung, M.-M. Wong, L.-H. Yung, Y.-W. Ho, W.-Y. Wong, D.-K.-P. Hau, R. Gambari, C.-H. Chui, The role of reactive oxygen species in the biological activity of antimicrobial agents: An updated mini review, Chem. Biol. Interact. 320 (2020) 109023, https://doi.org/10.1016/j.cbi.2020.109023;

c) F. Gao, T. Shao, Y. Yu, Y. Xiong, L. Yang, Surface-bound reactive oxygen species generating nanozymes for selective antibacterial action, Nat. Commun. 12 (2021) 745, https://doi.org/10.1038/s41467-021-20965-3.

[17] a) S. Razaviamri, K. Wang, B. Liu, B.P. Lee, Catechol-based antimicrobial polymers, Molecules 26 (2021) 559, https://doi.org/10.3390/molecules26030559;
b) Y.-S. Choi, H. Kang, D.-G. Kim, S.-H. Cha, J.-C. Lee, Mussel-inspired dopamine- and plant-based cardanol-containing polymer coatings for multifunctional filtration membranes, ACS Appl. Mater. Interfaces 6 (2014) 21297–21307, https://doi.org/10.1021/am506263s.

[18] a) L.-Y. Qu, J.-L. Liu, Y.-Y. Liu, G.-Q. Zhang, Y.-J. Xu, P. Zhu, Y.-Z. Wang, Anchoring silver nanoparticles using catechol-derived resins: An efficient and versatile approach for producing durable antimicrobial fabrics, Prog. Org. Coat. 176 (2023) 107397, https://doi.org/10.1016/j.porgcoat.2022.107397;
b) R. Bryaskova, N. Philipova, N. Georgiev, D. Ganchev, I. Lalov, C. Detrembleur, Bio-inspired antibacterial polymer coatings with included silver nanoparticles and porphyrin-based photosensitizer.J, Polym. Res. 30 (2023) 199, https://doi.org/10.1007/s10965-023-03572-2.

[19] a) B. Liu, J. Li, Z. Zhang, J.D. Roland, B.P. Lee, pH responsive antibacterial hydrogel utilizing catechol–boronate complexation chemistry, Chem. Eng. J. 441 (2022) 135808, https://doi.org/10.1016/j.cej.2022.135808;
b) N. Nazi, A. Marguier, C. Debiemme-Chouvy, V. Humblot, Optimization and antibacterial response of n-halamine coatings based on polydopamine, Colloids Interfaces 6 (2022) 9, https://doi.org/10.3390/colloids6010009.

[20] a) Y. Chen, X. Fan, J. Lu, X. Liu, J. Chen, Y. Chen, Mussel-inspired adhesive, antibacterial, and stretchable composite hydrogel for wound dressing, Macromol. Biosci. 23 (2022) 2200370, https://doi.org/10.1002/mabi.202200370;
b) F.J. Caro-León, M.L. López-Donaire, R. Vázquez, M. Huerta-Madroñal, J. Lizardi-Mendoza, W.M. Argüelles-Monal, D. Fernández-Quiroz, L. García-Fernández, J. San Roman, B. Vázquez-Lasa, P. García, M.R. Aguilar, DEAE/catechol–chitosan conjugates as bioactive polymers: synthesis, characterization, and potential applications, Biomacromolecules 24 (2023) 613–627, https://doi.org/10.1021/acs.biomac.2c01012;
c) L. Li, D. Chen, C. Yang, Y. Zeng, T. Jin, Y. Zhang, X. Sun, H. Mao, Z. Mu, X. Shen, Z. Ruan, X. Cai, Gelatin and catechol-modified quaternary chitosan cotton dressings with rapid hemostasis and high-efficiency antimicrobial capacity to manage severe bleeding wounds, Mater. Des. 229 (2023) 111927, https://doi.org/10.1016/j.matdes.2023.111927;
d) H. Lu, J. Liu, M. Yu, P. Li, W. Wu, Z. Hu, Y. Xiao, X. Xing, Photothermal-enhanced antibacterial and antioxidant hydrogel dressings based on catechol-modified chitosan-derived carbonized polymer dots for effective treatment of wound infections, Biomater. Sci. 10 (2022) 2692–2705, https://doi.org/10.1039/D2BM00221C.

[21] R. Pinnataip, B.P. Lee, Oxidation chemistry of catechol utilized in designing stimuli-responsive adhesives and antipathogenic biomaterials, ACS Omega 6 (2021) 5113–5118, https://doi.org/10.1021/acsomega.1c00006.

[22] S. Suárez-García, J. Sedó, J. Saiz-Poseu, D. Ruiz-Molina, Copolymerization of a catechol and a diamine as a versatile polydopamine-like platform for surface functionalization: the case of a hydrophobic coating, Biomimetics 2 (2017) 22, https://doi.org/10.3390/biomimetics2040022.

[23] a) Y. Zhang, S. Chen, J. An, H. Fu, X. Wu, C. Pang, H. Gao, Construction of an antibacterial membrane based on dopamine and polyethylenimine cross-linked graphene oxide, ACS Biomater. Sci. Eng. 5 (2019) 2732–2739, https://doi.org/10.1021/acsbiomaterials.9b00061;
b) X. He, E. Obeng, X. Sun, N. Kwon, J. Shen, J. Yoon, Polydopamine, harness of the antibacterial potentials-A review, Mater. Today Bio 15 (2022) 100329, https://doi.org/10.1016/j.mtbio.2022.100329;
c) D. Liu, H. Wang, X. Dong, X. Liu, S. Dosta, C. Zhang, P. Cao, Enhancing antibacterial and anticorrosion properties of 304 stainless steel surfaces: a multi-modification approach based on DA/PEI/SiO2/AMPs, J. Coat. Technol. Res. 20 (2023) 979–994, https://doi.org/10.1007/s11998-023-00806-2;
d) Y. Zhao, Y. Qian, H. Wang, W. Zhao, J. Zhao, H. Zhang, Bioinspired polycation functionalization of the polyurethane surface for enhanced lubrication, antibacterial property, and anticoagulation, ACS Appl. Polym. Mater. 5 (2023) 3999–4010, https://doi.org/10.1021/acsapm.3c00234;
e) M. Nakipoglu, A. Tezcaner, C.H. Contag, N. Annabi, N. Ashammakhi, Bioadhesives with antimicrobial properties, Adv. Mater. 2300840 (2023), https://doi.org/10.1002/adma.202300840.

[24] L. Canchy, D. Kerob, A.L. Demessant, J.-M. Amici, Wound healing and microbiome, an unexpected relationship, J. Eur. Acad. Dermatol. Venereol. 37 (2023) 7–15, https://doi.org/10.1111/jdv.18854.

[25] N. Fairley, V. Fernandez, M. Richard-Plouet, C. Guillot-Deudon, J. Walton, E. Smith, D. Flahaut, M. Greiner, M. Biesinger, S. Tougaard, D. Morgan, J. Baltrusaitis, Systematic and collaborative approach to problem solving using X-ray photoelectron spectroscopy, Appl. Surf. Sci. 5 (2021) 100112, https://doi.org/10.1016/j.apsadv.2021.100112.

[26] P. Thomas, A.C. Sekhar, R. Upreti, M.M. Mujawar, S.S. Pasha, Optimization of single plate-serial dilution spotting (SP-SDS) with sample anchoring as an assured method for bacterial and yeast cfu enumeration and single colony isolation from diverse samples, Biotech Rep. 8 (2015) 45–55, https://doi.org/10.1016/j.btre.2015.08.003.

[27] a) L. Jones, P. O'Shea, The electrostatic nature of the cell surface of candida albicans: a role in adhesion, Exp. Mycol. 18 (1994) 111–120, https://doi.org/10.1006/emyc.1994.1013;
b) W. Tian, F. Li, S. Wu, G. Li, L. Fen, X. Qu, X. Jia, Y. Wang, Efficient capture and T2 magnetic resonance assay of Candida albicans with inorganic nanoparticles: role of nanoparticle surface charge and fungal cell wall, ACS Biomater. Sci. Eng. 5 (2019) 3270–3278, https://doi.org/10.1021/acsbiomaterials.9b00069;
c) C. Teevan-Hanman, P. O'Shea, Candida albicans exhibit two classes of cell surface binding sites for serum albumin defined by their affinity, abundance and prospective role in interkingdom signalling, PLOS ONE 16 (2021), https://doi.org/10.1371/journal.pone.0254593.e0254593.

[28] a) H.-L. Cheah, V. Lim, D. Sandai, Inhibitors of the glyoxylate cycle enzyme ICL1 in Candida albicans for potential use as antifungal agents, PLOS ONE 9 (2014), https://doi.org/10.1371/journal.pone.0095951;
b) B.A.M. Cantelli, T.A. Bitencourt, T.T. Komoto, R.O. Beleboni, M. Marins, A. L. Fachin, Caffeic acid and licochalcone A interfere with the glyoxylate cycle of Trichophyton rubrum, Biomed. Pharmacother. 96 (2017) 1389–1394, https://doi.org/10.1016/j.biopha.2017.11.051.e95951.

[29] M.J. Esplandiu, N. Bastús, J. Fraxedas, I. Imhaz, V. Puntes, J. Radjenovic, B. Sepúlveda, A. Serrá, S. Suárez-García, G. Franzese, Interfacial phenomena in nanotechnological applications for water remediation, K. Wandelt, G. Bussetti, Encyclopedia of Solid-Liquid Interfaces 2024 Elsevier, Amsterdam, The Netherlands, 465–484, https://doi.org/10.1016/B978-0-323-85669-0.00066-0.